Journal of Pharmaceutical Analysis 11 (2021) 57–67

Contents lists available at ScienceDirect

Journal of Pharmaceutical Analysis

journal homepage: www.elsevier.com/locate/jpa

Original article

Bi_2O_3/ZnO nanocomposite: Synthesis, characterizations and its application in electrochemical detection of balofloxacin as an anti-biotic drug

Sana Ansari [a], M. Shahnawaze Ansari [b, c, d, *], Soami P. Satsangee [a, **], Rajeev Jain [e]

[a] Department of Chemistry, Dayalbagh Educational Institute, Dayalbagh, Agra, 282005, India
[b] Center of Nanotechnology, King Abdulaziz University, Jeddah, 21589, Saudi Arabia
[c] Advanced Membrane Technology Research Centre (AMTEC), Universiti Teknologi Malaysia, 81310, Skudai, Johor, Malaysia
[d] School of Chemical and Energy Engineering, Universiti Teknologi Malaysia, 81310, Skudai, Johor, Malaysia
[e] School of Studies in Chemistry, Jiwaji University, Gwalior, 474011, India

ARTICLE INFO

Article history:
Received 11 November 2019
Received in revised form
27 March 2020
Accepted 30 March 2020
Available online 4 April 2020

Keywords:
ZnO nanoparticles
Chemically modified electrode
Voltammetry
Drug analysis

ABSTRACT

In the present work, a chemically modified electrode has been fabricated utilizing Bi_2O_3/ZnO nanocomposite. The nanocomposite was synthesized by simple sonochemical method and characterized for its structural and morphological properties by using XRD, FESEM, EDAX, HRTEM and XPS techniques. The results clearly indicated co-existence of Bi_2O_3 and ZnO in the nanocomposite with chemical interaction between them. Bi_2O_3/ZnO nanocomposite based glassy carbon electrode (GCE) was utilized for sensitive voltammetric detection of an anti-biotic drug (balofloxacin). The modification amplified the electroactive surface area of the sensor, thus providing more sites for oxidation of analyte. Cyclic and square wave voltammograms revealed that Bi_2O_3/ZnO modified electrode provides excellent electrocatalytic action towards balofloxacin oxidation. The current exhibited a wide linear response in concentration range of 150−1000 nM and detection limit of 40.5 nM was attained. The modified electrode offered advantages in terms of simplicity of preparation, fair stability (RSD 1.45%), appreciable reproducibility (RSD 2.03%) and selectivity. The proposed sensor was applied for determining balofloxacin in commercial pharmaceutical formulations and blood serum samples with the mean recoveries of 99.09% and 99.5%, respectively.
© 2020 Xi'an Jiaotong University. Production and hosting by Elsevier B.V. This is an open access article under the CC BY-NC-ND license (http://creativecommons.org/licenses/by-nc-nd/4.0/).

1. Introduction

Fluoroquinolones are an important anti-bacterial group of drugs which have been developed recently and widely used for treatment of numerous bacterial infections [1]. Many newer fluoroquinolones have been used extensively for clinical purpose due to their broad spectra of activities and good oral absorption [2]. They are divided into four generations. The amendment of the drug to a suitable class is based on its pharmacological activity. Among various fluoroquinolones, balofloxacin (BLF) is a new fluoroquinolone which is chemically designated as 1-cyclopropyl-6-fluro-8-methoxy-7-(3-methylaminopiperidin-1-yl)-4-oxoquinoline-3-carboxylic acid. In its structure, the 7th place of fluoroquinolone ring is replaced with methylaminopiperidine and the 8th site is tailored with a methoxy group. BLF exhibits a broad antibacterial spectrum which lies in the range of gram-positive to gram-negative bacteria. It shows signs of admirable anti-bacterial action in opposition to gram-positive bacteria like multi-drug-resistant Staphylococci and Pneumococci. It gets metabolized in the kidneys to give glucuronide and N-des-methyl derivative [3].

Several analytical means have been developed to determine and analyze BLF in biological fluids and commercial dosages, such as high performance liquid chromatography (HPLC) [4,5], reverse phase-HPLC (RP-HPLC) [6], RP-HPLC coupled along fluorescence detector [7], HPLC-electrospray ionization mass spectroscopy [3] and UV-spectrophotometric method [8,9]. However, these techniques involve complicated preconcentration or multi-solvent extraction owing to the intricacy of real samples and small concentration of the analyte, usually time-consuming, and the need of expensive instrumentation and toxic solvents [10,11]. As compared

Peer review under responsibility of Xi'an Jiaotong University.
* Corresponding author. Center of Nanotechnology, King Abdulaziz University, Jeddah, 21589, Saudi Arabia.
** Corresponding author.
E-mail addresses: shah.csengg@gmail.com (M.S. Ansari), deiusic@gmail.com (S.P. Satsangee).

https://doi.org/10.1016/j.jpha.2020.03.013
2095-1779/© 2020 Xi'an Jiaotong University. Production and hosting by Elsevier B.V. This is an open access article under the CC BY-NC-ND license (http://creativecommons.org/licenses/by-nc-nd/4.0/).

to these techniques, electroanalytical systems have extensively been applied to study a broad range of drug molecules for their ease, less expenditure, and moderately little analysis time [12,13]. Additionally, with the help of electrochemistry one can elucidate the electrode mechanism [14]. Redox properties owned by organic molecules are able to provide insights into their metabolic outcome or in vivo redox progression or pharmacological activity. Another important benefit of electroanalytical methods is the use of chemically modified electrodes which are quite stable at ambient conditions and have been proved to overcome the disadvantages of using bare electrode [15,16].

To produce admirable sensors by means of chemically modified electrode, it is necessary to pursue appropriate electrode modification materials which possess superior electrical conductivity and better electrocatalytic ability [17]. Nowadays, electrode surface modification with nanostructure materials has been the focus of interest as it leads to amplification in electrochemical response of working electrode by enhancing the electron transport rate and reducing the overpotential for analyte detection. These electrodes significantly augment the selectivity in determination of drug molecules based on an electroanalytical approach [18].

Nanostructure metal oxides have brought in enormous interest for fabrication of electrochemical sensors for biological and pharmaceutical analysis [19–21]. Among metal oxides, zinc oxide (ZnO) nanoparticles have gained considerable attention for broad band gap (3.37 eV), large excitonic energy, no toxicity, good electron communication asset, good electrochemical activities and high mechanical strength [22]. In recent times, ZnO has been well thought-out as a hopeful material in terms of biosensor relevance for the reason that it has a higher isoelectric point (9.5) and biocompatible nature, and is abundantly present [23]. Due to these interesting properties, use of ZnO nanostructures has been reported for fabrication of electrochemical sensors and biosensors as reported in previous literature. Moyo et al. [22] discussed the electrochemical study of an anti-bacterial agent triclosan by merging the benefits of nano-zinc oxide and multiwalled carbon nanotubes (MWCNT). They reported higher oxidation current and reduced overpotential at nano-ZnO/MWCNT modified electrode. The detection limit achieved by them was 1.3 μg/L. The practical applicability was tested in tap water samples with acceptable recoveries. Karami and Sheikhshoaie [24] fabricated a tyrosine sensor using reduced graphene oxide (rGO) and ZnO as modifiers in carbon paste electrode. Square wave voltammograms revealed that presence of rGO/ZnO nanocomposite led to an increase in conductivity and hence the oxidation peak current. Tyrosine could be detected at its lowest limit of 0.07 μM and showed linear response in a wide concentration range of 0.1–400 μM. The sensor exhibited fair applicability for tyrosine detection in serum samples and water samples without interference from species like fructose, glucose, alanine, K^+, Br^-, and thiourea [24]. In another report by Karimi-Maleh et al. [25], simultaneous electrochemical determination was executed for levodopa and piroxicam at ZnO–Pd/CNTs modified glassy carbon electrode (GCE). The presence of nanocomposite escorted to improve the oxidation signal of levodopa by 70 times and piroxicam by 41.5 times due to its high conducting ability. Balasubramanian et al. [26] described electrochemical analysis of sulfamethoxazole (anti-biotic) using graphitic carbon nitride (g-C_3N_4) and ZnO nanocomposite which was prepared sonochemically. The sensor modified with g-C_3N_4/ZnO nanocomposite showed excellent electrocatalytic activity due to synergism between them. A detection limit of 6.6 nM was attained for sulfamethoxazone with practical ability in real samples. Unfortunately, some inherent characteristics of ZnO confine its broad-scale applications [27]. Therefore, to prevail over these flaws and accomplish improved electrocatalysis activity, ZnO is combined with other metal oxide nanomaterials to form mixed oxide nanocomposites. In particular, ZnO and Bi_2O_3 based nanocomposites have been reported to demonstrate distinct catalytic and electrical properties as a result of synergy between ZnO and Bi_2O_3 [28,29].

It is well known that Bi_2O_3 is a flexible material with an open array of applications owing to its small energy band gap (~2.1 V), superior surface area, fairly good conductor and photoconductivity [30,31]. The use of bismuth based nanoparticles as modifiers for electrode stimulated curiosity in the past decade for its excellent electron mobility [32]. Bi_2O_3 is also an environmentally-friendly material and a fine substitute of mercury in electrochemical analysis. Amongst a choice of metal oxides, bismuth oxide is proposed to boost the electroanalytical act of the sensors for determination of various metal ions and organic compounds including pharmaceutical drugs [33–36]. Thus, ZnO and Bi_2O_3 nanoparticles offer various functions for electroanalysis and are being reported to enhance the electrocatalytic and conducting properties due to their nanoscale dimensions, which assists the electrical contact between analyte and electrode surface. In view of this, high prospect of strengthening the electrochemical response in co-existence of both nanomaterials inspired us to combine ZnO and Bi_2O_3 and use the composite for electrode surface modification.

Considering the above discussion, the present paper reports the synthesis and characterization of Bi_2O_3/ZnO nanocomposite and fabrication of GCE with the nanocomposite to build up a novel voltammetric sensor for electrochemical determination of an antibiotic drug BLF. First, ZnO nanostructures were hydrothermally synthesized. Then, Bi_2O_3/ZnO nanocomposite was mixed via an ultrasonication approach. The Bi_2O_3/ZnO nanocomposite was proved to be responsible for enhancement in electrochemical oxidation of BLF in comparison to individual Bi_2O_3 and ZnO. To our finest understanding, no work has been reported on fabrication of GCE with Bi_2O_3/ZnO nanocomposite and its utilization for electrochemical analysis of BLF. Due to synergistic electrocatalytic activity of Bi_2O_3 and ZnO, this sensor offers a novel and proficient protocol for sensitive and selective analysis of drugs in pharmaceutical samples.

2. Experimental

2.1. Reagents and chemicals

BLF standard compound (99%, HPLC grade), zinc acetate anhydrous ($Zn(O_2CCH_3)_2$), cetyl trimethyl ammonium bromide (CTAB) and Bi_2O_3 nanoparticles were obtained from Sigma Aldrich Co. NaOH, absolute ethanol and dimethyl formamide (DMF) were purchased from Fisher Scientific (India). BLF tablets (B-Cin 50 mg) were purchased from a local pharmacy shop. A stock solution of 0.01 mM BLF was prepared with methanol in a 100 mL volumetric flask and kept at 4 °C. Working solutions were prepared freshly by transferring suitable aliquots from stock solution and diluting them with BR buffer solution [37]. All other aqueous solutions were configured in de-ionized water (18.2 MΩ·cm) generated from Elga purification system (UK). The reagents used in experimentation were of analytical grade quality and consumed with no additional refinement.

2.2. Synthesis of ZnO nanoparticles

In a usual synthesis procedure, 0.5 g of $Zn(O_2CCH_3)_2$ was added to 60 mL of saturated CTAB solution and was stirred for about 30 min. After that, 10 mL of 2 M NaOH solution was supplied and a white aqueous solution was formed. This resultant solution was moved into a Teflon lined vessel and set aside in an oven at 120 °C for 20 h. The product was subjected to several washings and

annealed at 500 °C for 2 h to obtain white powder of ZnO nanoparticles.

2.3. Characterizations

For phase detection of the prepared nanocomposite, X-ray diffraction (XRD) examination was made at room temperature on Rigaku Ultima IV diffractometer. The surface morphology and elemental analysis of the nanocomposite was examined through field emission scanning electron microscopy (FESEM) technique using Jeol JSM-7600F (Jeol, Japan) together with energy-dispersive X-ray spectrometer (EDAX) from Oxford Instruments (Japan). High-resolution transmission electron microscope technique (HRTEM) was executed on JEM-ARM200F (Jeol, Japan). Fourier Transform infrared (FTIR) was procured on a PerkinElmer FTIR spectrometer (UK) and X-ray photoelectron spectroscopy studies (XPS) were achieved on PHI5000Versa Probe II (PHI, USA).

2.4. Fabrication of GCE with Bi_2O_3/ZnO nanocomposite

For the preparation of nanocomposite, Bi_2O_3 and ZnO nanoparticles were dispersed in DMF at the ratio 1:1 (optimized). This dispersion was sonicated for a period of 2 h to get a homogenous suspension. At first, the surface of GCE was polished using 0.3 μm alumina slurry on a Buehler cloth and washed repeatedly until a clean and shiny surface appeared. Then, modified electrode was fabricated via simple drop-coating of 5 μL nanocomposite suspension on the surface and allowed to dry in air. A uniform coating of yellow color was formed on GCE surface and the resultant electrode was denoted as Bi_2O_3/ZnO/GCE. For comparison studies, Bi_2O_3/GCE and ZnO/GCE were also prepared individually.

2.5. Electrochemical measurements

All the electrochemical measurements including electrochemical impedance spectroscopy (EIS), cyclic voltammetry (CV) and square wave voltammetry (SWV) were executed on AUTOLAB-PGSTAT 302 N Potentiostat equipped with conventional 3-electrode cell assemblage with Pt wire (counter electrode), Ag/AgCl (reference electrode) and modified GCE (working electrode). The complete electrochemical set-up was provided by Metrohm (Switzerland). Before recording any measurement, pure N_2 gas was purged into solution containing BLF for a few minutes to get rid of any oxygen from the solution.

2.6. Preparation of samples for analysis (tablet sample and human blood serum sample)

The commercially obtainable B-Cin 50 mg were made into fine powder by grinding completely. Appropriate amount was weighed and dissolved in methanol, followed by sonication for 30 min. This solution was centrifuged and filtered to obtain a clear stock solution. Aliquots from this stock solution were further diluted with 0.2 M Britton-Robinson (BR) buffer to obtain the required concentrations of BLF working solution and proposed analytical procedure was applied for analysis of drug under optimum conditions.

The human blood serum sample was prepared by centrifugation for 15 min at 5000 rpm and then 1 mL of the supernatant was diluted further using 0.2 M BR buffer solution. Then aliquots from this solution were added to voltammetric cell for analysis. Three different concentrations were measured (100 nM, 300 nM and 500 nM) for recovery tests using SWV method.

3. Results and discussions

3.1. Structural and morphological characterizations

3.1.1. XRD analysis

The X-ray diffractogram of Bi_2O_3, ZnO and Bi_2O_3/ZnO nanocomposite is presented in Fig. 1. The XRD spectrum of Bi_2O_3 nanoparticles shows main diffraction peaks at 2θ = 27.9°, 30.3°, 31.8°, 32.7°, 46.28° and 55.56° corresponding to plane (201), (211), (002), (220), (222) and (421), respectively. The data can be well matched with JCPDS card number 01-078-1793 for tetragonal structure of β-Bi_2O_3. For the as-synthesized ZnO nanoparticles, XRD pattern shows diffraction peaks at 2θ = 31.7°, 34.4°, 36.2°, 47.5°, 56.5°, 62.8°, 66.3°, 67.9°, 69.1°, 72.5°, 76.9°, 81.3° and 89.6°, which can be indexed to planes (100), (002), (101), (102), (110), (103), (200), (112), (201), (004), (202), (104) and (203), respectively. No additional peaks were noticed in the diffraction pattern of ZnO, thus confirming formation of pure ZnO nanoparticles. The pattern corresponds to hexagonal zincite structure matching well with JCPDS card number 01-075-7917. In XRD pattern of Bi_2O_3/ZnO nanocomposite, spectrum shows the diffraction peaks of both Bi_2O_3 and ZnO nanoparticles. This confirms the successful formation of Bi_2O_3/ZnO nanocomposite. As observed, the diffraction pattern of nanocomposite is shifted to a minute extent with slight changes in lattice as compared to pure Bi_2O_3 and ZnO nanoparticles. This might be due to interaction between components in the composite. To further calculate the average crystallite size, Debye Scherrer equation was used [38] as shown below:

$$D = \frac{K\lambda}{FWHM\ (Cos\ \theta)} \quad (1)$$

where K is a dimensionless number of the order of unity, known as the Scherrer constant. Its actual value depends on no less than three factors: the definition of "breadth", the crystallite shape and the crystallite-size distribution [39]. λ is the X-ray wavelength (CuKα = 1.54 Å), *FWHM* is the full width at half maxima of highest

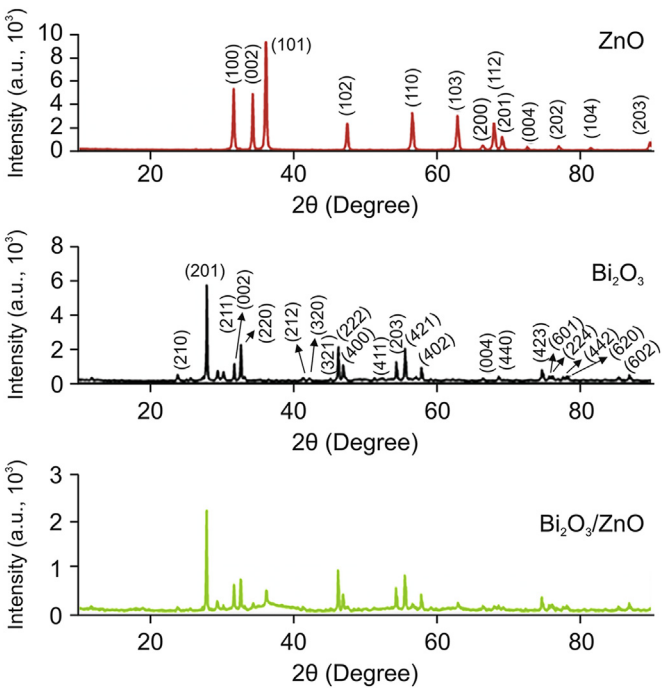

Fig. 1. XRD pattern of ZnO, Bi_2O_3 and Bi_2O_3/ZnO nanocomposite.

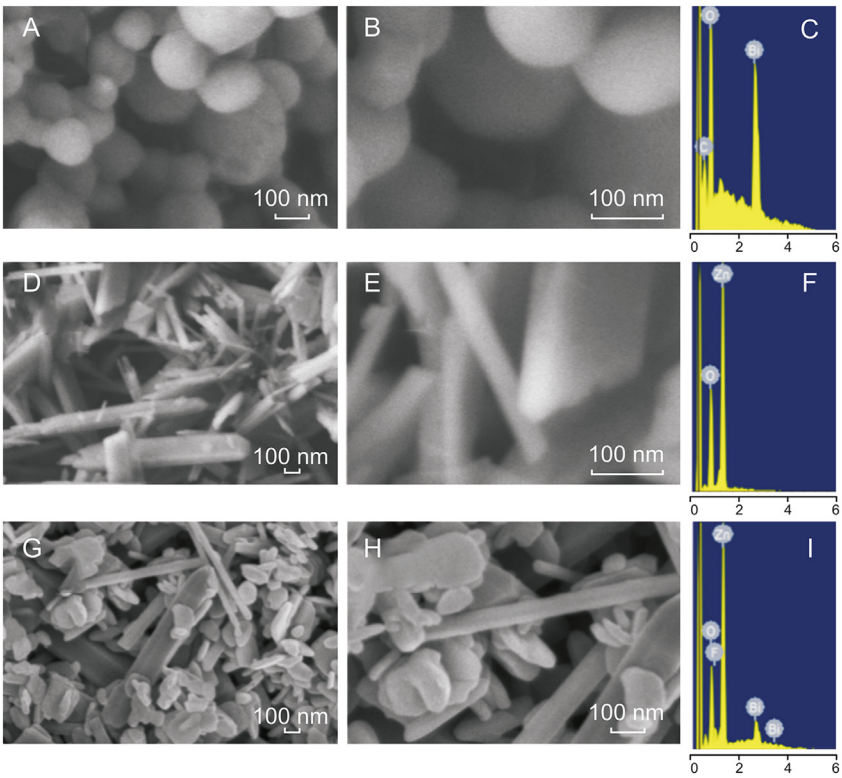

Fig. 2. Low magnification, high magnification FESEM image, and EDAX spectra of (A–C) Bi_2O_3 nanoparticles, (D–F) ZnO nanoparticles, and (G–I) Bi_2O_3/ZnO nanoparticles.

intensity signal (in radians) and θ corresponds to Bragg's angle (in degrees). Using the above equation, the average crystallite size of Bi_2O_3, ZnO nanoparticles and Bi_2O_3/ZnO nanocomposite was found to be 77.8 nm, 39.7 nm and 46 nm, respectively.

3.1.2. FESEM and EDAX analysis

The structural and morphological investigations of the prepared materials were carried out using FESEM as shown in Fig. 2. The micrographs were obtained at two different magnifications (low and high magnification) for each material. Figs. 2A and B (low and high magnification images) show FESEM micrographs of Bi_2O_3 nanoparticles with spherical morphology having particles size in the range of 90–210 nm. EDAX graph of the same confirmed the presence of only Bi and O in their elemental form (Fig. 2C). From Figs. 2D and E, the surface structure of the as-synthesized ZnO can be observed where disks and rod type structures are present having a diameter in nano-range but the length up to a few microns. Fig. 2F shows EDAX spectrum with Zn and O as elements, thus indicating synthesis of pure ZnO nanoparticles. Interestingly, on formation of nanocomposite, we obtained a difference in morphological characteristics as compared to individual components as shown in Figs. 2G and H. We observed that Bi_2O_3 nanoparticles are well distributed among ZnO rods and disks. However, it was also noticed that Bi_2O_3 spheres had lost their sole geometry. Formation of nanocomposite was further evidenced from EDAX spectrum (Fig. 2I) and elemental composition (Table 1), which demonstrates the existence of Bi, Zn and O as elements, indicating high purity of the products.

Table 1
Elemental composition of Bi_2O_3/ZnO nanocomposite.

Element	Weight (%)	Atomic (%)
O K	11.17	39.73
F K	2.90	8.68
Zn L	47.16	41.04
Bi M	38.76	10.55
Totals	**100.00**	

3.1.3. HRTEM analysis

Typical TEM and HRTEM images along with selected area electron diffraction (SAED) patterns of Bi_2O_3 nanoparticles and Bi_2O_3/ZnO nanocomposite are exposed in Fig. 3. Fig. 3A shows TEM image of Bi_2O_3 nanoparticles with a spherical shape while the HRTEM image, as shown in Fig. 3B, depicts the lattice fringes with d-spacing of 3.45 Å corresponding to (210) plane of β-Bi_2O_3. Fig. 3D displays the morphology of Bi_2O_3/ZnO nanocomposite where we can clearly see the existence of nearly spherical nanoparticles of Bi_2O_3 surrounded with some disks and rod like nanostructures of ZnO. Further, the HRTEM image (Fig. 3E) shows interface between Bi_2O_3 and ZnO nanostructures with sub-atomic resolution where atom-to-atom spacing (d-spacing) of 3.45 Å for β-Bi_2O_3 and 2.60 Å for ZnO can be seen. So, the composite material consists of both Bi_2O_3 and ZnO nanostructures. The SAED patterns for Bi_2O_3 (Fig. 3C) and Bi_2O_3/ZnO (Fig. 3F) show that both samples are polycrystalline in nature. It is clearly visible in the SAED patterns of Bi_2O_3 nanostructures that the d-spacing is a bit larger, which is in well agreement of its HRTEM image, whereas in Fig. 3F, the existence of two different ranges of d-spacing corresponding to, β phase of Bi_2O_3 spheres and ZnO disks and rods, is an indication for the formation of Bi_2O_3/ZnO nanocomposite.

3.1.4. FTIR analysis

In addition, the functional interaction between Bi_2O_3 and ZnO nanoparticles was further exemplified using FTIR technique. Fig. 4 shows FTIR spectrum of ZnO nanoparticles showing band around

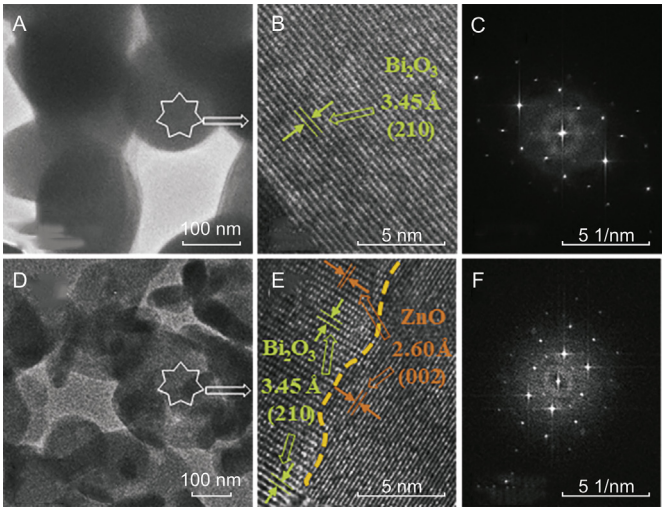

Fig. 3. TEM, HRTEM, and SAED pattern of (A–C) Bi_2O_3 nanoparticles, and (D–F) Bi_2O_3/ZnO nanocomposite.

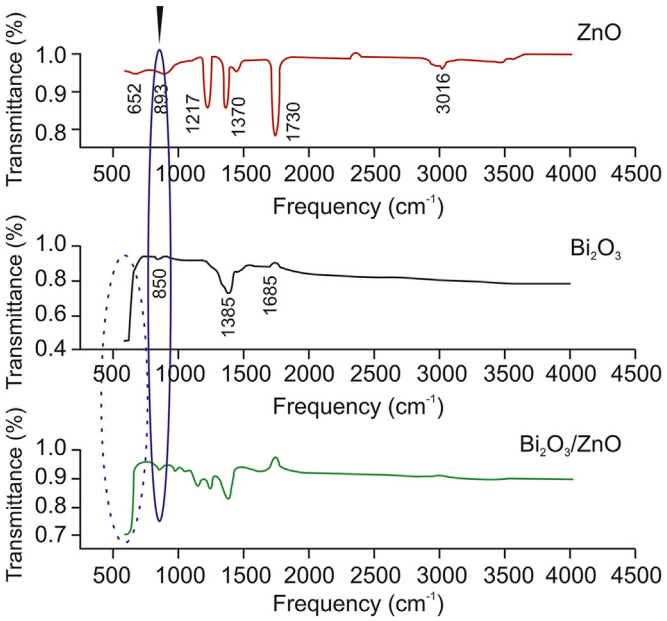

Fig. 4. FTIR spectra of ZnO, Bi_2O_3 and Bi_2O_3/ZnO nanocomposite.

652 cm^{-1}, which is due to Zn–O–Zn anti-symmetric and symmetric stretching vibrations. The band observed at 893 cm^{-1} arises owing to stretching vibration of Zn–OH of ZnO. The peak appearing at 3016 cm^{-1} is due to O–H stretching vibrations of absorbed H_2O molecules [40]. The additional peaks appearing at 1217 and 1730 cm^{-1} can be ascribed to the stretching vibrations of C–O and C=O of the absorbed CO_2 molecules [41]. In FTIR spectrum of Bi_2O_3 nanoparticles, band was observed at 850 cm^{-1}, which was credited to stretching mode of vibrations in Bi–O–Bi. The peaks observed in the range of 400–600 cm^{-1} and at 1385 cm^{-1} are characteristic of Bi_2O_3. The FTIR spectrum of Bi_2O_3/ZnO nanocomposite also shows bands in the region of 400–600 cm^{-1} which corresponds to metal-oxygen-metal (M-O-M) vibrations [42]. Furthermore, the characteristic peaks of the two metal oxides (Bi_2O_3 and ZnO) can be clearly seen from the spectrum with shifts in peak intensities, which indicate that there is interaction between the two metal oxides resulting in the formation of nanocomposite successfully.

3.1.5. XPS analysis

XPS study was implemented to establish the presence of elements and valence states in Bi_2O_3 and Bi_2O_3/ZnO nanocomposites. The complete scan XPS spectrum (Fig. 5A) confirms the occurrence of Zn 2p, Bi 4f and O 1s core levels. Fig. 5B shows Bi 4f high-resolution XPS spectrum for Bi_2O_3, where signals at 158.5 eV and 163.8 eV can be ascribed to Bi^{3+} $4f_{7/2}$ and Bi^{3+} $4f_{5/2}$, respectively [43]. The O 1s spectrum for Bi_2O_3 can be deconvoluted into three signals as shown in Fig. 5C. The spectrum reflects the most intense peak at 531.7 eV which corresponds to Bi–O bond while the signal at 532.8 eV is associated with surface adsorbed molecules [44].

In case of Bi_2O_3/ZnO nanocomposite, Bi 4f high resolution XPS spectrum (Fig. 5D) shows the above mentioned two peaks (158.5 eV and 163.8 eV) with slight upward shift at 159 eV and 164.1 eV, respectively [43]. This positive shift might be indicative of the existence of strong interactions between ZnO and Bi_2O_3 nanostructures [45,46]. This might be attributed to fractional electron transfer from Bi to ZnO. A similar phenomenon is also reported in other literature [47,48]. There are two small signals at 157.7 eV and 162.9 eV, which are ascribed to Bi^0 $4f_{7/2}$ and Bi^0 $4f_{5/2}$, respectively [49]. Therefore, small amount of bismuth is present in its metallic form along with Bi^{3+} chemical state. The O 1s spectrum (Fig. 5E) for Bi_2O_3/ZnO nanocomposite sample shows three signals at binding energy values, 529.7 eV for lattice oxygen in ZnO (O–Zn^{2+}), the signal at 530.9 eV corresponds to oxygen in Bi_2O_3 (O–Bi^{3+}) and the peak appearing at higher binding energy values of 532 eV, is due to surface adsorbed oxygen species. The peak profiles and binding energies of Zn^{2+} were observed from Fig. 2F, where Zn $2p_{3/2}$ and Zn $2p_{1/2}$ in the composite material occur at 1021.8 eV and 1044.9 eV, respectively. The entire spectra encompass a shift downward of 0.6 eV as compared to the typical peak site of Zn $2p_{3/2}$ at 1022.4 eV [43]. The signals are endorsed to the lattice zinc in ZnO. Thus, the characterization results including XRD, FESEM, HRTEM, FTIR along with XPS tool are evident for the existence of ZnO and Bi_2O_3 nanoparticles in the composite.

3.2. Electrochemical characterizations

3.2.1. Role of surface area and impedance

CV was employed to investigate the redox behavior of Bi_2O_3/ZnO nanocomposite modified sensor using 1 mM $K_3Fe(CN)_6$ (0.1 M KCl) as a redox probe. Fig. S1A shows cyclic voltammograms of bare GCE, Bi_2O_3/GCE, ZnO/GCE and Bi_2O_3/ZnO/GCE at 0.05 V/s scan rate. At bare GCE, two well defined oxidation and reduction peaks were observed, and the peak current values increased further at Bi_2O_3/GCE and ZnO/GCE. However, a remarkable enhancement in current values was noticed at Bi_2O_3/ZnO/GCE along with negative shift in peak potential. This clearly demonstrates that Bi_2O_3/ZnO/GCE acts as an efficient electron transfer mediator.

To calculate the electroactive surface area (A) at bare and each modified GCE, Randles Sevcik equation was used as displayed below [50]:

$$I_p = 2.69 \times 10^5 \, AD^{1/2} n^{3/2} v^{1/2} C \quad (2)$$

Here A = electroactive surface area (in cm^2), C = concentration of $K_3[Fe(CN)_6]$ (in mol/cm^3), the number of electrons transferred is denoted by symbol n which is 1 for $K_3[Fe(CN)_6]$, D stands for diffusion coefficient which is 7.65 × 10^{-6} cm^2/s for $K_3[Fe(CN)_6]$ and v is the scan rate (V/s). Cyclic voltammograms were witnessed at varying scan rates (0.01–0.1 V/s) for Bi_2O_3/ZnO/GCE as shown in Fig. S1B and from the slope of graph of I_p vs. $v^{1/2}$ (Inset of Fig. S1B), A

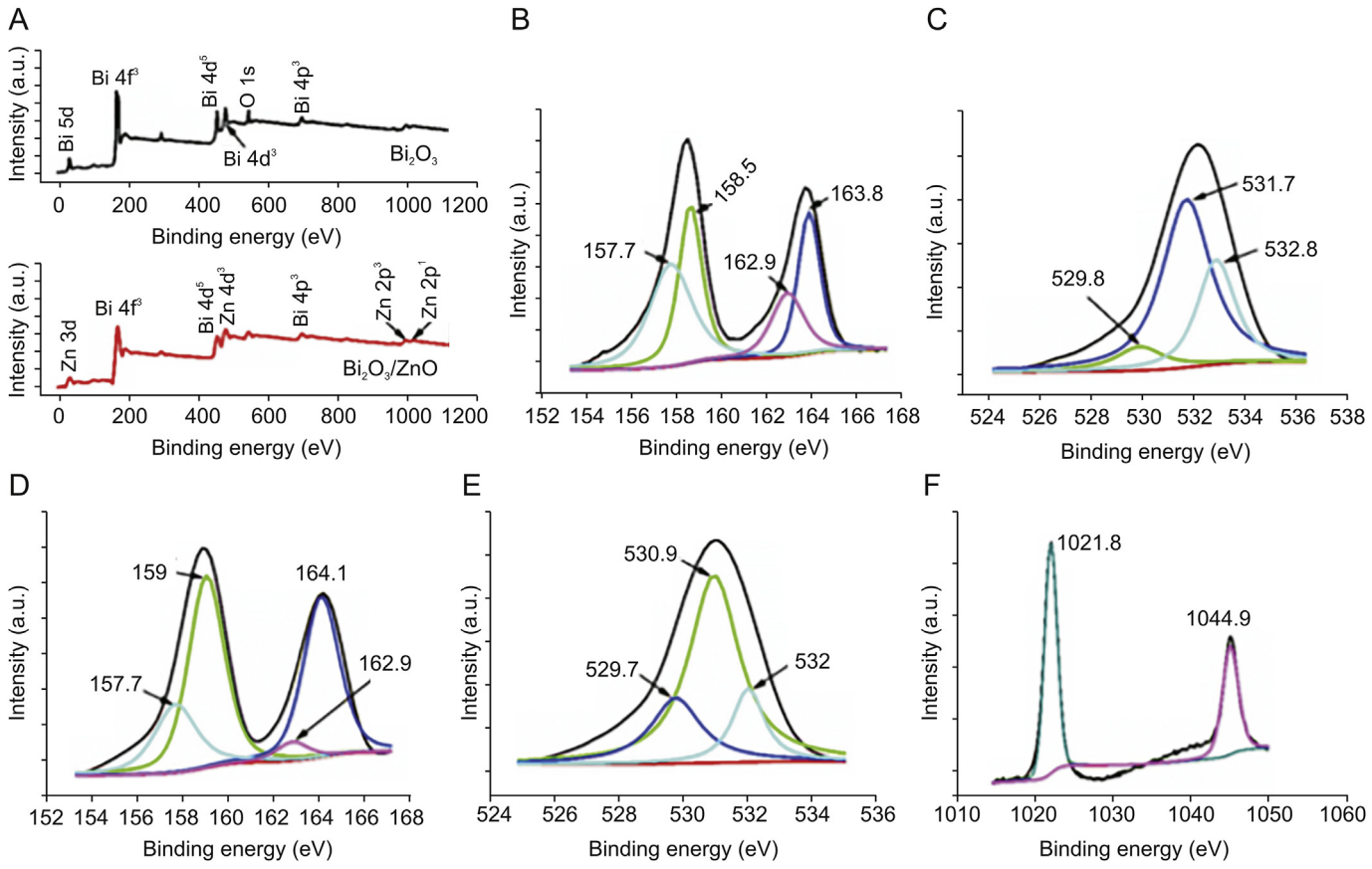

Fig. 5. (A) XPS survey spectra of Bi_2O_3 and Bi_2O_3/ZnO, (B, C) XPS core level spectra of Bi 4f, and O 1s in Bi_2O_3, and (D–F) XPS core level spectra of Bi 4f, O 1s, and Zn 2p in Bi_2O_3/ZnO sample.

was calculated to be 0.027, 0.054, 0.081 and 0.27 cm^2 for bare GCE, Bi_2O_3/GCE, ZnO/GCE and Bi_2O_3/ZnO/GCE, respectively. Thus, we see that the electroactive surface area is amplified by 10 times at nanocomposite modified GCE in contrast to bare GCE.

Experiments were further extended to employ EIS measurements using 5 mM K_3[Fe (CN)$_6$] solution. To examine the capacity of electron transfer at each electrode, we obtained the Nyquist plots as shown in Fig. 6. The higher frequency region in these plots represents a depressed semi-circle while the lower frequency region shows a linear portion with somewhat slight curve. The electrical circuits compatible with Nyquist plots are displayed as Inset in Fig. 6 which consisted of four elements, namely, solution resistance (R_s), double layer capacitance (Q_{dl}), charge transfer resistance (R_{CT}) and Warburg impedance (W). The depressed semi-circle region in Nyquist plots is associated with charge transfer resistance and the linear portion represents diffusion limited process. On observing Nyquist plots, we see that the semi-circle portion is the largest for bare GCE and the least for Bi_2O_3/ZnO/GCE. Thus, charge transfer resistance offered by nanocomposite modified sensor got reduced owing to its conducting behavior. Further, values of R_{ct} were evaluated and found to be 14.6, 8.85, 7.10 and 4.04 kΩ for bare GCE, Bi_2O_3/GCE, ZnO/GCE and Bi_2O_3/ZnO/GCE, respectively.

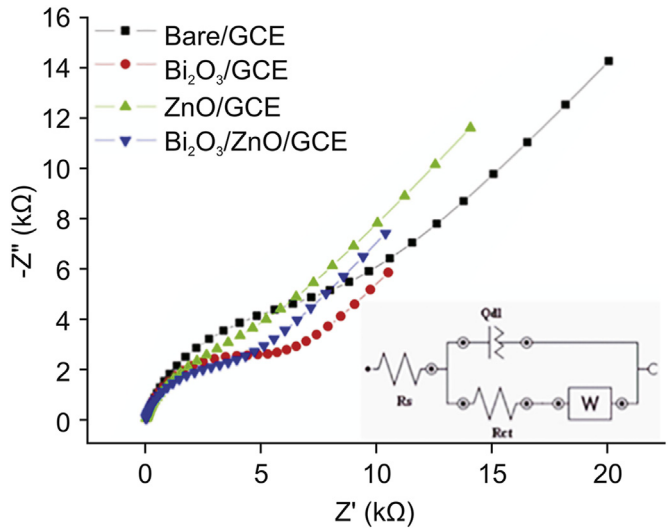

Fig. 6. Nyquist plots from EIS at bare GCE, Bi_2O_3/GCE, ZnO/GCE and Bi_2O_3/ZnO/GCE in 5 mM K_3 [Fe (CN)$_6$] in 0.1 M KCl solution. Inset: Corresponding equivalent circuit [Rs (Q [Rct W])].

3.2.2. Electrochemical behavior of BLF at Bi_2O_3/ZnO/GCE

To determine the role of individual material and the possible synergism between them, cyclic and square wave voltammograms were recorded at bare GCE, Bi_2O_3/GCE, ZnO/GCE and Bi_2O_3/ZnO/GCE in 0.2 M BR buffer (pH 4.5) for 300 nM of BLF. Fig. 7A shows cyclic voltammogram of BLF with an irreversible oxidation peak which increases successively from bare, Bi_2O_3, and ZnO to Bi_2O_3/ZnO/GCE. Thus, it is obvious that oxidation peak current was higher at Bi_2O_3/ZnO/GCE as compared to bare and other modified electrodes. These results can also be verified by analyzing Fig. 7B, which shows square wave voltammograms of BLF at each electrode. This

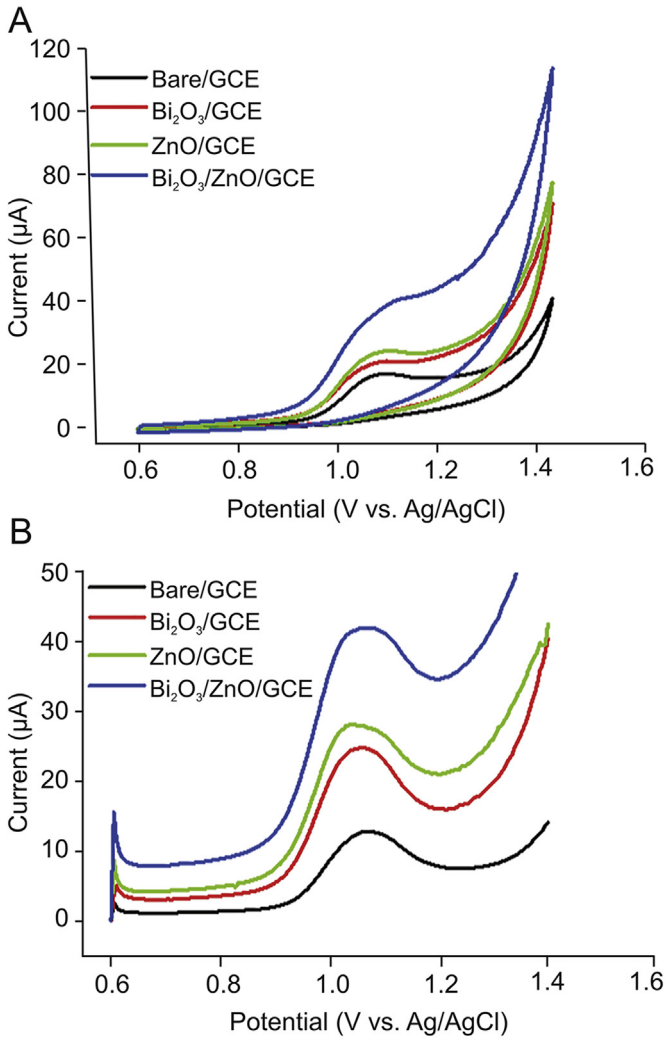

Fig. 7. (A) Cyclic voltammograms and (B) square wave voltammograms for determination of BLF (300 nM) at pH 4.5 in 0.2 M BR buffer at bare GCE and modified GCE.

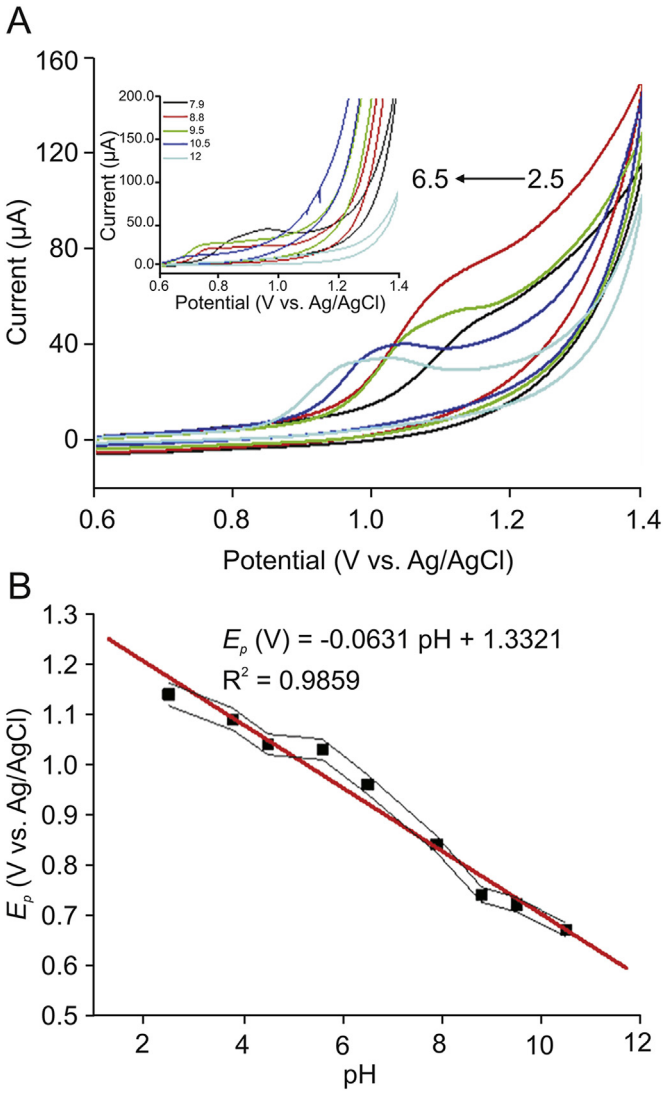

Fig. 8. (A) Cyclic voltammograms of 300 nM BLF in 0.2 M BR buffer at Bi_2O_3/ZnO/GCE at varying pH values (2.5–6.5); Inset: Cyclic voltammograms of 300 nM BLF in 0.2 M BR buffer at Bi_2O_3/ZnO/GCE at varying pH values (7.9–12). (B) Plot of E_p (V) vs. pH values.

significant enhancement in current at Bi_2O_3/ZnO/GCE can be ascribed to synchronized overture of Bi_2O_3 and ZnO nanoparticles, which also divulged the subsistence of synergistic effects in the Bi_2O_3/ZnO/GCE electrode. These synergistic actions can be related to the increased superficial area and excellent electron transfer abilities of ZnO and Bi_2O_3 nanoparticles. Moreover, addition of ZnO nanoparticles provided higher conductivity due to the existence of oxygen vacancies and other donor type point defects [51]. Therefore, the electron transfer of BLF on Bi_2O_3/ZnO/GCE increased.

3.2.3. *Effect of pH*

The pH of solution is an imperative chemical factor as it changes the reduction and oxidation potential of the analytes, gives information regarding involvement of protons in surface reaction between the electrode material and analyte. Therefore, pH dependency on electrochemical behavior of 300 nM BLF at Bi_2O_3/ZnO/GCE was explored in 0.2 M BR buffer in pH range of 2.5–12. Fig. 8A shows the cyclic voltammogram for influence of pH on analyte oxidation potential and peak current. We can see that the peak potential shifted negatively with respect to increment in pH values, which indicates that protons are occupied in oxidation process of BLF at Bi_2O_3/ZnO/GCE. The BLF exhibited a good oxidation signal at pH 4.5 which was chosen as optimum pH for further experimental investigations. In addition, peak potential (E_p) vs. pH plot was drawn as shown in Fig. 8B and the linear regression equation can be presented as:

$$E_p(\mathrm{V}) = -0.0631\mathrm{pH} + 1.3321 \quad \left(R^2 = 0.9859\right) \tag{3}$$

As observed, the peak potential of BLF illustrates a linear relation with pH and moves towards more negative potentials with a slope of about 63.1 mV/pH. The obtained experimental value lies in close proximity with Nernstian value of 59 mV, which is suggestive of an equivalent number of electrons and protons participating in charge transfer process [52].

3.2.4. *Influence of scan rate*

The oxidative behavior of BLF at Bi_2O_3/ZnO/GCE was studied by investigating the effect of scan rate variation (5–100 mV/s) on oxidation peak current of BLF. Valuable information could be gained using the relationship of peak current and scan rate. Fig. S2A shows that oxidation peak current (I_p) improved progressively with the

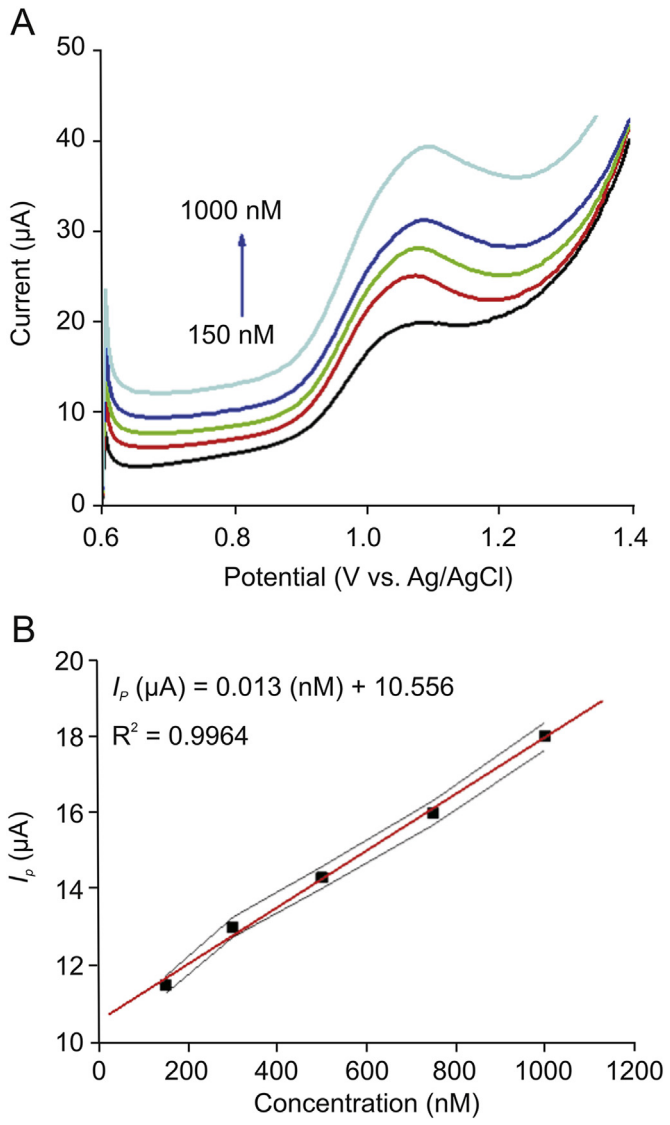

Fig. 9. (A) Square wave voltammograms of BLF at different concentrations (150–1000 nM) in 0.2 M BR buffer at pH 4.5. (B) Plot of I_p (μA) vs. concentration (nM).

increase in scan rate (v) and a linear relation was obtained between I_p and $v^{1/2}$ (Fig. S2B). The regression equation can be given as:

$$I_p(\mathrm{A}) = 69.573\, v^{1/2}(\mathrm{V/s}) - 4.3899 \quad \left(R^2 = 0.9938\right) \tag{4}$$

This indicates that the electrochemical behavior of BLF at Bi_2O_3/ZnO/GCE is a diffusion process. To further confirm this, a plot of log I_p and log v was obtained as shown in Fig. S2C which gave a linear relationship with regression equation as shown below:

$$\log I_p(\mu\mathrm{A}) = 0.705 \log v(\mathrm{V/s}) + 2.1535 \quad \left(R^2 = 0.9985\right) \tag{5}$$

For a diffusion peak, the slope value must be 0.5 and for an adsorption peak it must be 1, but here we obtained an intermediate slope value of 0.7, which suggests a mixed diffusion-adsorption process [53].

Further, we observed an up-shift in peak potential (E_p) with rising scan rate and we plotted a linear graph between E_p and log v (Fig. S2D) which can be expressed as:

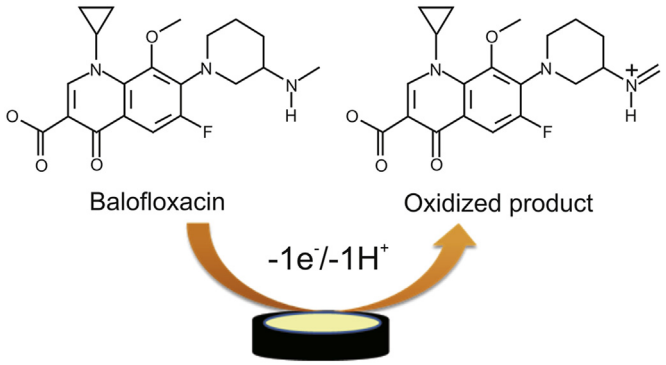

Scheme 1. Plausible oxidation mechanism of balofloxacin.

$$E_p(\mathrm{V}) = 0.1045 \log v \ (\mathrm{V/s}) + 1.1401 \quad \left(R^2 = 0.9912\right) \tag{6}$$

According to Laviron's equation [54], relationship between E_p and ν can be described as follows:

$$E_p = \mathrm{E}^0 + \left(\frac{2.303\ \mathrm{RT}}{\alpha \mathrm{nF}}\right)\log\left(\frac{\mathrm{RTk}^0}{\alpha \mathrm{nF}}\right) + \left(\frac{2.303\ \mathrm{RT}}{\alpha \mathrm{nF}}\right)\log v \tag{7}$$

where E° is the formal redox potential, α stands for transfer coefficient, k° is the standard rate constant of the reaction in s^{-1} and n is the number of electrons involved in electrode reaction. From the slope of E_p versus log v, the value of αn was calculated to be 0.56. Typically, for a complete irreversible diffusion-controlled electrode process, we assume α value to be 0.5. Bard et al. [55] equation was used for calculation of α.

$$\alpha = \frac{47.7}{E_p - E_p/2} \tag{8}$$

Using the above equation, α was calculated to be 0.63 which is close to the theoretical value and this value relates to a diffusion-controlled irreversible anodic process. In turn, the number of electrons was also calculated using Eq. (1) and was found to be ≈ 1. In the outlook, proportions of electrons to protons concerned in the reactions was calculated approximately as 1:1. Thus, we can say that 1 electron and 1 proton were transferred in the oxidation of BLF at Bi_2O_3/ZnO/GCE. Based on above results, a plausible oxidation mechanism has been proposed for BLF (Scheme 1) [56].

3.2.5. Analytical performance and method validation of Bi_2O_3/ZnO/GCE

In order to see the practicability of the investigated method for the quantification of BLF, the relationship between oxidative peak current and concentration was assessed using SWV technique at Bi_2O_3/ZnO/GCE. As shown in Fig. 9A, peak current response increased by raising the concentration and a linear correlation was acquired between peak current and concentration over the range of 150–1000 nM (Fig. 9B), which obeys the following linear regression equation:

$$I_p(\mu\mathrm{A}) = 0.013\ (\mathrm{nM}) + 10.556 \quad \left(R^2 = 0.9964\right) \tag{9}$$

The limit of detection (LOD) was calculated using 3 S/m and limit of quantification (LOQ) was estimated as 3 S/m. Here, S represents standard deviation and m represents slope of calibration plot. Thus, LOD was found as 40.5 nM with sensitivity of 12.85 nA/nM and LOQ was found to be 135 nM. The present work has also been compared with other analytical methods in terms of LOD and

Table 2
Comparison of the present method with other reported methods.

Method	LOD	Linear range	Refs.
HPLC-electrospray ionization (ESI)-MS	0.02 μg/mL	0.03–3 μg/mL	[3]
RP-HPLC-fluorescence	0.078 μg/mL	0.078–20.00 μg/mL	[57]
IL-DLLME followed by the HPLC method	0.01 μg/mL	0.04–10.0 μg/mL	[58]
Bi_2O_3/ZnO/GCE	**40.5 nM or 15.77 ng/mL**	**150–1000 nM**	**This work**

linearity range of concentration (Table 2) [3,57,58]. It can be concluded that the present work offers LOD and working linearity comparable to other methods.

The developed method was validated in terms of reproducibility, stability and interference. To estimate the reproducibility and stability of the Bi_2O_3/ZnO/GCE sensor, four individual electrodes were fabricated under identical conditions, and experienced for the electrochemical detection of 300 nM BLF in 0.2 M BR buffer (pH 4.5) utilizing SWV technique. A relative standard deviation (RSD) of 2.03% was attained with four different electrodes, validating that the preparation of the electrode had significant reproducibility. In addition, to illustrate the repeatability of the prepared Bi_2O_3/ZnO/GCE electrode, six recurring measurements were conceded in presence of 300 nM BLF. The RSD of voltammetric responses on the Bi_2O_3/ZnO/GCE was 2.12% (Table 3).

Additionally, long-term stability tests over a 2-week period were taken using prepared electrode. The Bi_2O_3/ZnO/GCE was stored up in a desiccated place at room temperature (25 °C) and the voltammetric results confirmed that peak current response of the modified electrode lost only 4% of the initial current response with RSD 1.45% after storage for 2 weeks. These results designate that Bi_2O_3/ZnO/GCE has good reproducibility and stability; thus the proposed method is satisfactory for BLF determination.

The possible interferences of some inorganic ions, vitamins and amino acids on the determination of 300 nM BLF were studied by SWV. The results showed that 500-fold surplus of ordinary ions like Na^+, Ca^{2+}, K^+, CO_3^{2-} and NO_3^- and 200-fold excess of common excipients, such as glucose, starch, lactose, sucrose, ascorbic acid, gum acacia, uric acid, folic acid, pyridoxine and cobalamine did not interfere with the determination of BLF and signal changes observed were less than 5%, indicating that the proposed electrode is highly selective (Table 4).

Table 3
Reproducibility and repeatability results at Bi_2O_3/ZnO/GCE in presence of 300 nM BLF.

Sensor	Sensor reproducibility	
	Average current (μA)	RSD (%)
Sensor I	13.04[a]	1.87
Sensor II	13.56[a]	2.04
Sensor III	12.87[a]	2.23
Sensor IV	13.34[a]	1.99
Average	13.20[b]	2.03

[a] Average of six replicates.
[b] Average of four sensors.

Table 4
Influence of excipients on oxidation behavior of BLF.

Foreign species	Concentration (μM)	Signal change (%)
Glucose	60	1.05
Starch	60	−1.32
Lactose	60	−0.14
Sucrose	60	0.63
Ascorbic acid	60	3.7
Gum Acacia	60	2.80
Uric acid	60	0.83
Folic acid	60	−1.9
Pyridoxine	60	1.45
Cobalamine	60	1.3
Na^+	150	−1.87
Ca^{2+}	150	−1.2
K^+	150	−1.49
CO_3^{2-}	150	2.79
NO_3^-	150	1.3

3.2.6. Analytical application (B-Cin tablet and blood serum sample)

The present research is provoked to prepare an electrode material for real sample analysis. Hence, the Bi_2O_3/ZnO/GCE sensor was exposed for real sample studies using BLF tablets and human blood serum. BLF contents were determined in formulation B-Cin 50 mg. The sample preparation is described in Experimental section. Three different concentrations were prepared as 100, 300 and 500 nM. Then, recovery tests were carried out by transferring each into the electrochemical cell and standard addition method was applied at optimal parameters using SWV method. The obtained results summarized in Table 5 displayed that the sensor shows exceptional recovery with RSD less than 2%. Hence, the method is reliable for direct determination of BLF.

4. Conclusions

A novel and simple strategy for the selective and sensitive determination of BLF at Bi_2O_3/ZnO/GCE is presented in this work. The results from characterization studies including XRD, FESEM, HRTEM, and FTIR along with XPS tool are evident for the existence of ZnO and Bi_2O_3 nanoparticles in the composite with chemical

Table 5
Determination of BLF in pharmaceutical tablet and human blood serum using the proposed method at Bi_2O_3/ZnO/GCE.

Sample	Standard added (nM)	Standard found[b] (nM)	Recovery (%)[a]	RSD (%)
B-Cin tablet (50 mg)	100	98.73 ± 0.47	98.73	0.81
	300	298.8 ± 0.77	99.6	0.39
	500	494.8 ± 0.63	98.96	0.59
Blood serum	100	99.12 ± 1.23	99.12	0.91
	300	296.7 ± 0.66	98.9	0.32
	500	501.9 ± 1.02	100.4	0.75

[a] [standard found/standard added] × 100.
[b] Amount found represents the average of six observations ($n = 6$).

interactions between them. From all the electrochemical results, the Bi_2O_3/ZnO nanocomposite was found to have high electrocatalytic activity towards BLF oxidation with reduction in overpotential and enhancement in current signals, which can be ascribed to synchronized overture of Bi_2O_3 and ZnO nanoparticles. The main advantages of the present study are the ease of fabrication of electrode, its reproducibility, selectivity and achievement of low LOD. The present study did not involve much use of chemicals. Most of the solutions were made in aqueous solvents. But it was also noticed that the sensor displayed good stability for two weeks. The fabricated electrode provided a lower electron transfer resistance (R_{ct}=4.04 kΩ) and high surface area (0.27 cm^2), which promoted a faster electron transfer process. A wide linear response was exhibited by Bi_2O_3/ZnO/GCE in the concentration range of 150–1000 nM with detection limit of 40.5 nM and sensitivity of 12.85 nA/nM. The sensor showed less than 5% signal change in the presence of various interfering species. In addition, the developed sensor was applied to BLF tablets and human blood serum for practical application and was proved to be a good sensing platform for real sample analysis.

Declaration of competing interest

The authors declare that there are no conflicts of interest.

Acknowledgments

The authors express their gratitude to the University Grants Commission (UGC) for providing Maulana Azad National Fellowship for minority students.

Appendix A. Supplementary data

Supplementary data to this article can be found online at https://doi.org/10.1016/j.jpha.2020.03.013.

References

[1] G. Schmuck, A. Schürmann, G. Schlüter, Determination of the excitatory potencies of fluoroquinolones in the central nervous system by an in vitro model, Antimicrob. Agents Chemother. 42 (1998) 1831–1836.
[2] Y. Ni, Y. Wang, S. Kokot, Simultaneous determination of three fluoroquinolones by linear sweep stripping voltammetry with the aid of chemometrics, Talanta 69 (2006) 216–225.
[3] Z. Bian, Y. Tian, Z. Zhang, et al., High performance liquid chromatography–electrospray ionization mass spectrometric determination of balofloxacin in human plasma and its pharmacokinetics, J. Chromatogr. B 850 (2007) 68–73.
[4] T. Nakagawa, M. Ishigai, Y. Hiramatsu, et al., Determination of the new fluoroquinolone balofloxacin and its metabolites in biological fluids by high performance liquid chromatography, Arzneim. Forsch. 45 (1995) 716–718.
[5] J. Deng, Z. Xiao, H. Zhang, et al., Determination of balofloxacin in human plasma by HPLC with solid-phase extraction, Chinese J. Chromatography 25 (2007) 942–943.
[6] N. Nyola, J. Govindasamy, Estimation of balofloxacin in active pharmaceutical ingredient and pharmaceutical formulations by different analytical methods, Nov. Sci. Int. J. Pharmaceut. Sci. 1 (2012) 425–429.
[7] Y. Sui, T. Guo, J.-w. Zhang, et al., Determination of balofloxacin in human urine by RP-HPLC with fluorescence detection, J. Shenyang Pharmaceut. Univ. 24 (2007) 691–694.
[8] M. Punam, B. Vandana, Development and validation of analytical methods for estimation of balofloxacin in bulk and pharmaceutical dosage forms, Int. J. PharmTech. Res. 3 (2011) 1938–1941.
[9] S.A. Reddy, K.C. Sekhar, Development and validation of analytical method for estimation of balofloxacin in bulk and pharmaceutical dosage form, J. Global Trends Pharmaceut. Sci. 3 (2012) 647–655.
[10] R. Jain, V.K. Gupta, N. Jadon, et al., Voltammetric determination of cefixime in pharmaceuticals and biological fluids, Anal. Biochem. 407 (2010) 79–88.
[11] M.L. Yola, V.K. Gupta, T. Eren, et al., A novel electro analytical nanosensor based on graphene oxide/silver nanoparticles for simultaneous determination of quercetin and morin, Electrochim, Acta 120 (2014) 204–211.
[12] R.N. Goyal, V.K. Gupta, A. Sangal, et al., Voltammetric determination of uric acid at a fullerene-C60-modified glassy carbon electrode, Electroanalysis 17 (2005) 2217–2223.
[13] H. Karimi-Maleh, O.A. Arotiba, Simultaneous determination of cholesterol, ascorbic acid and uric acid as three essential biological compounds at a carbon paste electrode modified with copper oxide decorated reduced graphene oxide nanocomposite and ionic liquid, J. Colloid Interface Sci. 560 (2020) 208–212.
[14] T. Bančič, J. Bitenc, K. Pirnat, et al., Electrochemical performance and redox mechanism of naphthalene-hydrazine diimide polymer as a cathode in magnesium battery, J. Power Sources 395 (2018) 25–30.
[15] M. Govindasamy, S.M. Chen, V. Mani, et al., Molybdenum disulfide nanosheets coated multiwalled carbon nanotubes composite for highly sensitive determination of chloramphenicol in food samples milk, honey and powdered milk, J. Colloid Interface Sci. 485 (2017) 129–136.
[16] V. Mani, M. Govindasamy, S.-M. Chen, et al., Determination of dopamine using a glassy carbon electrode modified with a graphene and carbon nanotube hybrid decorated with molybdenum disulfide flowers, Microchim. Acta 183 (2016) 2267–2275.
[17] M. Miraki, H. Karimi-Maleh, M.A. Taher, et al., Voltammetric amplified platform based on ionic liquid/NiO nanocomposite for determination of benserazide and levodopa, J. Mol. Liq. 278 (2019) 672–676.
[18] E. Tammari, A. Nezhadali, S. Lotfi, et al., Fabrication of an electrochemical sensor based on magnetic nanocomposite Fe_3O_4/β-alanine/Pd modified glassy carbon electrode for determination of nanomolar level of clozapine in biological model and pharmaceutical samples, Sens. Actuators B Chem. 241 (2017) 879–886.
[19] S. Ansari, M.S. Ansari, H. Devnani, et al., CeO_2/g-C_3N_4 nanocomposite: a perspective for electrochemical sensing of anti-depressant drug, Sens. Actuators B Chem. 273 (2018) 1226–1236.
[20] H. Devnani, S. Ansari, S.P. Satsangee, et al., ZrO_2-Graphene-Chitosan nanocomposite modified carbon paste sensor for sensitive and selective determination of dopamine, Mater. Today Chem. 4 (2017) 17–25.
[21] S. Ansari, M.S. Ansari, S. Satsangee, et al., WO_3 decorated graphene nanocomposite based electrochemical sensor: a prospect for the detection of anti-anginal drug, Anal. Chim, Acta 1046 (2019) 99–109.
[22] M. Moyo, L.R. Florence, J.O. Okonkwo, Improved electro-oxidation of triclosan at nano-zinc oxide-multiwalled carbon nanotube modified glassy carbon electrode, Sens. Actuators B Chem. 209 (2015) 898–905.
[23] J. Wang, X.W. Sun, A. Wei, et al., Zinc oxide nanocomb biosensor for glucose detection, Appl. Phys. Lett. 88 (2006), 233106.
[24] Z. Karami, I. Sheikhshoaie, rGO/ZnO nanocomposite modified carbon paste electrode as sensor for tyrosine analysis, Anal. Bioanal. Electrochem. 9 (2017) 834–840.
[25] H. Karimi-Maleh, I. Sheikhshoaie, A. Samadzadeh, Simultaneous electrochemical determination of levodopa and piroxicam using a glassy carbon electrode modified with a ZnO–Pd/CNT nanocomposite, RSC Adv. 8 (2018) 26707–26712.
[26] P. Balasubramanian, R. Settu, S.M. Chen, et al., Voltammetric sensing of sulfamethoxazole using a glassy carbon electrode modified with a graphitic carbon nitride and zinc oxide nanocomposite, Microchim. Acta 185 (2018), 396.
[27] H. Lv, G. Ji, Z. Yang, et al., Enhancement photocatalytic activity of the graphite-like C_3N_4 coated hollow pencil-like ZnO, J. Colloid Interf. Sci 450 (2015), 381–387.
[28] S. Balachandran, M. Swaminathan, Facile fabrication of heterostructured Bi_2O_3–ZnO photocatalyst and its enhanced photocatalytic activity, J. Phys. Chem. C 116 (2012) 26306–26312.
[29] S. Yi, X. Yue, D. Xu, et al., Study on photogenerated charge transfer properties and enhanced visible-light photocatalytic activity of p-type Bi_2O_3/n-type ZnO heterojunctions, New J. Chem. 39 (2015) 2917–2924.
[30] L. Li, B. Yan, $BiVO_4$/Bi_2O_3 submicrometer sphere composite: microstructure and photocatalytic activity under visible-light irradiation, J. Alloys Compd. 476 (2009) 624–628.
[31] S. Manavalan, U. Rajaji, S.-M. Chen, et al., Sonochemical synthesis of bismuth (III) oxide decorated reduced graphene oxide nanocomposite for detection of hormone (epinephrine) in human and rat serum, Ultrason. Sonochem. 51 (2019) 103–110.
[32] I. Svancara, C. Prior, S.B. Hocevar, et al., A decade with bismuth-based electrodes in electroanalysis, Electroanalysis 22 (2010) 1405–1420.
[33] N.L. Teradal, J. Seetharamappa, Bulk modification of carbon paste electrode with Bi_2O_3 nanoparticles and its application as an electrochemical sensor for selective sensing of anti-HIV drug nevirapine, Electroanalysis 27 (2015) 2007–2016.
[34] É.S. Sá, P.S. da Silva, C.L. Jost, et al., Electrochemical sensor based on bismuth-film electrode for voltammetric studies on vitamin B2 (riboflavin), Sens. Actuators B Chem. 209 (2015) 423–430.
[35] G. Bia, L. Borgnino, P.I. Ortiz, et al., Multivariate optimization of square wave voltammetry using bismuth film electrode to determine atrazine, Sens. Actuators B Chem. 203 (2014) 396–405.
[36] D. Asbahr, L.C.S. Figueiredo-Filho, F.C. Vicentini, et al., Differential pulse adsorptive stripping voltammetric determination of nanomolar levels of methotrexate utilizing bismuth film modified electrodes, Sens. Actuators B Chem. 188 (2013) 334–339.
[37] S.D. Bukkitgar, N.P. Shetti, R.M. Kulkarni, Construction of nanoparticles composite sensor for atorvastatin and its determination in pharmaceutical and urine samples, Sens. Actuators B Chem. 255 (2018) 1462–1470.

[38] A.L. Patterson, The scherrer formula for X-ray particle size determination, Phys. Rev. 56 (1939) 978–982.
[39] J.I. Langford, A. Wilson, Scherrer after sixty years: a survey and some new results in the determination of crystallite size, J. Appl. Crystallogr. 11 (1978) 102–113.
[40] R.S.J. Thomas, Solar light driven photocatalytic degradation of organic pollutants using ZnO nanorods coupled with photosensitive molecules, J. Environ. Chem. Eng 5 (2017) 4239–4250.
[41] M. Stan, A. Popa, D. Toloman, et al., Antibacterial and antioxidant activities of ZnO nanoparticles synthesized using extracts of allium sativum, rosmarinus officinalis and ocimum basilicum, acta metall, Sin.-Engl 29 (2016) 228–236.
[42] A. Hezam, K. Namratha, Q.A. Drmosh, et al., Synthesis of heterostructured Bi_2O_3–CeO_2–ZnO photocatalyst with enhanced sunlight photocatalytic activity, Ceram. Int. 43 (2017) 5292–5301.
[43] J.F. Moulder, W.F. Stickle, P.E. Sobol, Handbook of X-Ray Photoelectron Spectroscopy, Phys. Electron (1995) 230–232.
[44] S. Kang, R.C. Pawar, Y. Pyo, et al., Size-controlled BiOCl–RGO composites having enhanced photodegradative properties, J. Exp. Nanosci. 11 (2016) 259–275.
[45] A. Hashemi, A. Bahari, Synthesis and characterization of silanized-SiO_2/povidone nanocomposite as a gate insulator: the influence of Si semiconductor film type on the interface traps by deconvolution of Si_{2s}, Curr. Appl. Phys. 18 (2018) 1546–1552.
[46] A. Hashemi, A. Bahari, S. Ghasemi, Synthesis and characterization of cross-linked nanocomposite as a gate dielectric for p-type silicon field-effect transistor, J. Electron. Mater. 47 (2018) 3717–3726.
[47] J. Zhu, S. Wang, J. Wang, et al., Highly active and durable Bi_2O_3/TiO_2 visible photocatalyst in flower-like spheres with surface-enriched Bi_2O_3 quantum dots, Appl. Catal. B Environ. 102 (2011) 120–125.
[48] S. Yi, X. Yue, D. Xu, et al., Study on photogenerated charge transfer properties and enhanced visible-light photocatalytic activity of p-type Bi_2O_3/n-type ZnO heterojunctions, New J. Chem. 39 (2015) 2917–2924.
[49] H. Gnayem, Y. Sasson, Nanostructured 3D sunflower-like bismuth doped $BiOCl_xBr_{1-x}$ solid solutions with enhanced visible light photocatalytic activity as a remarkably efficient Technology for water purification, J. Phys. Chem. C 119 (2015) 19201–19209.
[50] A.J. Bard, L.R. Faulkner, Electrochemical Methods: Fundamentals and Applications, 2nd Edition, John Wiley & Sons Inc., Hoboken, 2001, pp. 386–428.
[51] J. Tashkhourian, B. Hemmateenejad, H. Beigizadeh, et al., ZnO nanoparticles and multiwalled carbon nanotubes modified carbon paste electrode for determination of naproxen using electrochemical techniques, J. Electroanal. Chem. 714–715 (2014) 103–108.
[52] Y. Wei, M. Li, S. Jiao, et al., Fabrication of CeO_2 nanoparticles modified glassy carbon electrode and its application for electrochemical determination of UA and AA simultaneously, Electrochim. Acta 52 (2006) 766–772.
[53] D.K. Gosser. Cyclic Voltammetry: Simulation and Analysis of Reaction Mechanisms, Jr VCH, New York, 1993.
[54] E. Laviron, General expression of the linear potential sweep voltammogram in the case of diffusionless electrochemical systems, J. Electroanal. Chem. Interfacial Electrochem. 101 (1979) 19–28.
[55] A.J. Bard, L.R. Faulkner, J. Leddy, et al., Electrochemical Methods: Fundamentals and Applications, Wiley, New York, 1980.
[56] M.M. Baizer, Organic Electrochemistry: An Introduction and a Guide, Marcel Dekker, New York, 1973.
[57] D.W. Wang, L. Xie, J. Wang, et al., Determination of balofloxacin in plasma by HPLC-Fluorescence and its pharmacokinetics in rats, J. China Pharmaceut. Univ. 35 (2004) 160–163.
[58] R.N. Rao, C.G. Naidu, C.V. Suresh, et al., Ionic liquid based dispersive liquid–liquid microextraction followed by RP-HPLC determination of balofloxacin in rat serum, Anal. Methods 6 (2014) 1674–1683.